Engineering with Computers
https://doi.org/10.1007/s00366-018-0678-3

ORIGINAL ARTICLE

A multivariate normal boundary intersection PCA-based approach to reduce dimensionality in optimization problems for LBM process

Gabriela Belinato[1,2] · Fabrício Alves de Almeida[1] · Anderson Paulo de Paiva[1] · José Henrique de Freitas Gomes[1] · Pedro Paulo Balestrassi[1] · Pedro Alexandre Rodrigues Carvalho Rosa[3]

Received: 25 July 2018 / Accepted: 7 December 2018

Abstract
Laser beam machining (LBM) is a promising manufacturing process that exhibits several desirable quality characteristics. Given a large number of objective functions, the level of complexity increases in an optimization problem. Therefore, this study presents a multivariate application of the normal boundary intersection (NBI) method to reduce dimensionality in optimization problems of the LBM process. Such an approach is capable of exploring the entire solution space with only a small number of Pareto points, and generating equispaced frontiers based on the objective functions written in terms of principal component scores. Hence, a design of experiment with three input parameters and six quality characteristics was undertaken to appropriately model the process requirements applied to AISI 314S steel. The results indicate that the proposed methodology is capable of achieving optimal values for interest characteristics. In addition, this approach shows a reduction in computational effort of approximately 91.89% (from 259 to 21 subproblems) in obtaining the best solution for rough operation.

Keywords Laser beam machining · Principal component analysis · Normal boundary intersection · Material removal rate · Roughness

1 Introduction

Manufacturing processes, such as machining processes, present many critical quality characteristics, such as various types of roughness, as well as performance and productivity characteristics. Among the machining processes, the laser beam machining (LBM) process is prevalent as a promising and non-consumable method. LBM is a non-conventional method that exhibits several industrial advantages [1], in addition to being widely applicable in automotive, civil, and nuclear sectors [2]. This process has high potential for applications in precision mechanics and micromechanics, but the expansion is being postponed due to a high initial investment cost and the high energy consumption involved in the process. This difficulty causes the number of published studies to be reduced, limiting the information on the appropriate parameters to allow optimization of the manufacturing process, either the rate of removal of material or the finish of the roughness surfaces. Many studies of multiobjective applications can be found in the literature, such as [3–8], however the LBM process is not very exploited.

Machining processes are, in general, considered as multiobjective problems once they involve more than one performance characteristic. LBM processes involve important input parameters, each of which is crucial in the process. Some of the main parameters are the following: laser frequency (f), cutting speed (S), laser power (I), pulse intensity, [9]. The main quality characteristics investigated in LBM are the material removal rate (MRR), roughness, and metallurgical and mechanical properties [2].

Electronic supplementary material The online version of this article (https://doi.org/10.1007/s00366-018-0678-3) contains supplementary material, which is available to authorized users.

✉ Fabrício Alves de Almeida
fabricio.alvesdealmeida@gmail.com

[1] Institute of Industrial Engineering and Management, Federal University of Itajubá, Itajubá, Brazil

[2] IFSULDEMINAS Federal Institute of South Minas Gerais, Pouso Alegre, Brazil

[3] IDMEC Department of Mechanical Engineering, Technician Superior Institute of Lisbon, University of Lisbon, Lisbon, Portugal

Published online: 12 December 2018

An advantage of the LBM process, compared to other types of machining processes, is that the material removal is performed without contact with the workpiece. This material removal from the workpiece is machined with precision and minimal dispersion, in addition to the non-use of consumables (tool wear). In the LBM process, the basic material removal mechanism is performed from the energy absorption of the laser in front of a series of pulses directed at the same point. The laser beam interacts thermally with the workpiece and when the laser beam focuses on the workpiece surface, an interaction occurs followed by a thermal reaction [10, 11]. During this interaction, the laser energy is transformed into thermal energy. The thermal energy intensity increases with each beam pulse. Thus, the surface temperature increases rapidly until the workpiece material starts to melt and vaporize; consequently, the material is removed layer by layer.

LBM can be performed on a wide range of materials [12, 13]. The laser beam interaction is different in metallic and non-metallic materials. In metallic materials, the laser focus dissolves and vaporizes the surface of the material through thermal reaction; this is known as metal sublimation. However, in non-metallic materials such as polymers, the laser interaction can break the molecular chains, which is a process known as laser ablation [14]. For this study, we will use a metallic material that is AISI 314S stainless steel, that was used in previous studies [15, 16].

Laser beam is used widely in cutting [11], drilling [10], micromachining [10, 17–20], and welding [21, 22]. Lasers can also be used to perform turning and milling operations [2]. Most of the input parameters affect the dimensional accuracy and product quality directly. Thus, it is necessary to establish the appropriate process parameters to satisfy the conflicting objectives of this process simultaneously [23]. The quality of the laser-machined workpieces can be improved through the proper optimization and control of various process parameters [11]. For optimization applications, many previous machining studies use strategies such as the design of experiment (DOE) [24]. The DOE is a statistical technique used to reduce experimental costs, to model and optimize the experiments [24–26]. The response surface methodology (RSM) is a DOE typically used in manufacturing, with applicability in several processes [27]. The DOE strategy is also used in LBM process studies, such as Taguchi design [9, 17, 28] and RSM [29, 30]. From all RSM designs, Almeida et al. [24] highlighted the central composite design (CCD) capable of generating complete quadratic models.

LBM demonstrates many interesting characteristics such as roughness and MRR that can be influenced by the input parameters. The DOE techniques aim to plan the parameters accurately for an experimental process and minimize algorithms optimization computational work. Several studies have used the RSM to model machine parameters in LBM and other machining processes [20, 31, 32].

In processes that present several quality characteristics, such as LBM, a significant correlation may exist between those characteristics. In this case, the variance–covariance data structure must be considered. To analyze multicorrelated response adequately, it is necessary to use multivariate strategies, such as the principal component analysis (PCA). This technique considers and analyzes multivariate data and can reduce the dimensionality of the problem. Hence, the iterations, subproblem numbers, and computational effort of the algorithms can be minimized.

Considering the characteristics presented in this process, this work aims to perform the optimization of the LBM process using multivariate techniques such as PCA to reduce the computational effort of optimization problems and, consequently, to consider the variance–covariance structure of this process [33]. The application will be performed in AISI 314S stainless steel and the optimization process will be conducted by the normal boundary intersection (NBI) method, which is a multiobjective optimization algorithm capable of generating balanced and equidistant Pareto frontiers. Figure 1 illustrates how the proposed procedure will be performed, through an Ishikawa diagram.

This paper is organized as follows: Sect. 2 presents the theoretical background describing the strategies of RSM, PCA, and the multiobjective optimization by the NBI method used in his work; Sect. 3 describes the materials and methods used; Sect. 4 presents the application, method, results, technical discussion and confirmation runs; Sect. 5 presents the comparisons with NBI without the PCA strategy; finally, Sect. 6 draws the conclusion.

2 Theoretical background

2.1 Response surface methodology

RSM is a technique that aims to optimize a certain response [34, 35]; its implementation is easy and economical [36], and it does not require many experimental runs [37]. Equation (1) shows the second-order polynomial that represents the response surface [24, 38]:

$$Y = \beta_0 + \sum_{i=1}^{k} \beta_i x_i + \sum_{i=1}^{k} \beta_{ii} x_i^2 + \sum_{i<j} \sum \beta_{ij} x_i x_j + \varepsilon, \tag{1}$$

where Y are the responses, x the parameters, β the estimated coefficients, k the number of independent variables, and ε the associated error term.

According to Montgomery [34], a CCD is the most frequently used array to fit second-order models. A

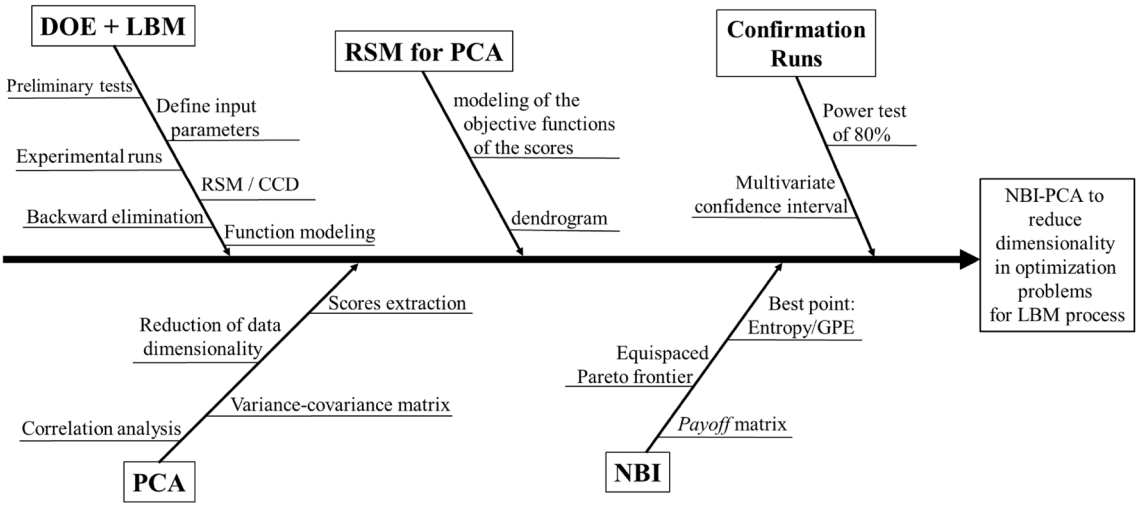

Fig. 1 Ishikawa diagram for the methods applied in this study

CCD is composed of 2^k factorial, $2k$ axial, and c_p center points, and is used widely in machining applications, such as those reported in [24, 39–43]. In addition, CCD presents greater advantages than other types of design [34]. A geometrical representation of the CCD is shown in Fig. 2.

2.2 Principal component analysis

In manufacturing processes with multiple responses, using univariate techniques may not be favorable owing to the multivariate response nature. Therefore, it is more appropriate to use multivariate techniques. PCA is a multivariate analysis technique that minimizes data dimensionality and can represent several correlated responses in a small number of uncorrelated latent variables [32].

According to Johnson and Wichern [44], when objective functions $f_1(\boldsymbol{x}), f_2(\boldsymbol{x}), \ldots, f_p(\boldsymbol{x})$ are correlated in terms of the aleatory vector $Y^T = [Y_1, Y_2, \ldots, Y_p]$ and $\boldsymbol{\Sigma}$ is the variance–covariance matrix associated to this vector, $\boldsymbol{\Sigma}$ can be divided by eigenvalues and eigenvectors $(\lambda_i, e_i), \ldots, \geq (\lambda_p, e_p)$, where $(\lambda_1 \geq \lambda_1 \geq \ldots \geq \lambda_p \geq 0)$, and ith is the non-correlated linear combination designated by $\mathrm{PC}_1 = e_i^T Y = e_1^T Y_1 + e_2^T Y_2 + \ldots + e_p^T Y_p$, with $i = 1,2,\ldots,p$. The ith principal component (PC) can be obtained by

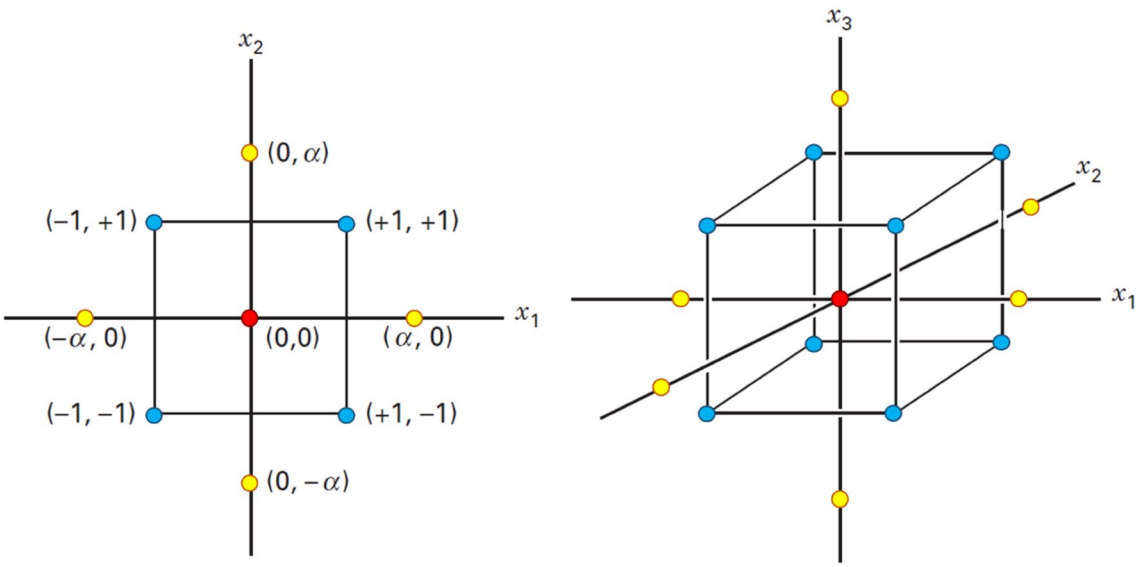

Fig. 2 CCD geometric representation for $k = 2$ and $k = 3$. Adapted from [34]

maximizing the linear combination. A set of original variables can be replaced by uncorrelated linear combinations in the PC form and can be expressed in terms of a matrix [44]. Such dimensionality reduction favors optimization techniques, presenting better computational modeling and more accurate results.

2.3 Normal boundary intersection

The NBI method, proposed by [45], is a multiobjective optimization approach capable of obtaining equispaced Pareto-optimal solutions [46], superior to the method of weighted sums [27, 47, 48]. The NBI mathematical formulation can be written as in Eq. 2.

$$\begin{aligned} &\underset{(\mathbf{x},t)}{\text{Max}} \; t \\ &S.t: \; \overline{\mathbf{\Phi}}\boldsymbol{\beta} + t\hat{\mathbf{n}} = \overline{\mathbf{F}}(\mathbf{x}) \\ &\mathbf{x} \in \Omega \\ &g_j(x) \leq 0 \\ &h_j(x) = 0, \end{aligned} \tag{2}$$

where $\mathbf{\Phi}$ represents the payoff matrix, obtained by the individual optimization of each objective function; $\overline{\mathbf{\Phi}}$ is the scaled payoff matrix; $\boldsymbol{\beta}$ refers to the weight vector for each utopia point; t is a scalar that is perpendicular to the utopia line. $\hat{\mathbf{n}}$ is the normal vector and $\overline{\mathbf{F}}(\mathbf{x})$ represents the vector of the dimensioned objective functions. In the payoff matrix ($\mathbf{\Phi}$) and scaled payoff matrix ($\overline{\mathbf{\Phi}}$), the ith line consists of the minimum and maximum values of the $f_i\,(x)$ function [46, 47].

The Utopia point is the vector that contains the individual optimum $f^U = \left[f_1^*(x_1^*), \ldots, f_i^*(x_i^*), \ldots, f_m^*(x_m^*)\right]^T$. It is the best possible value but is typically outside the viable solution region. On the contrary, the Nadir point contains the non-optimum value of each objective function and is the worst possible solution $f^N = \left[f_1^N, \ldots, f_i^N, \ldots, f_m^N\right]^T$ [34]. The payoff matrices are described by Eq. (3):

$$\mathbf{\Phi} = \begin{bmatrix} f_1^*(x_1^*) & \cdots & f_1(x_i^*) & \cdots & f_1(x_m^*) \\ \vdots & \ddots & & & \vdots \\ f_i(x_1^*) & \cdots & f_i^*(x_i^*) & \cdots & f_i^*(x_m^*) \\ \vdots & & & \ddots & \vdots \\ f_m(x_1^*) & \cdots & f_m(x_i^*) & \cdots & f_m^*(x_m^*) \end{bmatrix} \Rightarrow \overline{\mathbf{\Phi}} = \begin{bmatrix} \bar{f}_1^*(x_1^*) & \cdots & \bar{f}_1(x_i^*) & \cdots & \bar{f}_1(x_m^*) \\ \vdots & \ddots & & & \vdots \\ \bar{f}_i(x_1^*) & \cdots & \bar{f}_i^*(x_i^*) & \cdots & \bar{f}_i^*(x_m^*) \\ \vdots & & & \ddots & \vdots \\ \bar{f}_m(x_1^*) & \cdots & \bar{f}_m(x_i^*) & \cdots & \bar{f}_m^*(x_m^*) \end{bmatrix}, \tag{3}$$

where $\bar{f}_i(\mathbf{x}) = \left[\frac{f_i(\mathbf{x}) - f_i^U}{f_i^N - f_i^U}\right] = \left[\frac{f_i(\mathbf{x}) - f_i^I}{f_i^{MAX} - f_i^I}\right]$.

Therefore, for bi-objective problems, the NBI formulation of Eq. (2) can be rewritten as in Eq. (4):

$$\begin{cases} \underset{\mathbf{x}}{Min} \;\; F(\mathbf{x}) = \bar{f}_1(x) \\ St.: \bar{f}_1(\mathbf{x}) - \bar{f}_2(\mathbf{x}) + 2\beta_1 - 1 = 0 \\ \mathbf{x} \in \Omega \\ g_j(\mathbf{x}) \leq 0 \\ h_{j+1}(x) = 0 \end{cases}. \tag{4}$$

2.4 Entropy and global percentage error (GPE)

In front of a Pareto frontier, it is necessary to choose the best point to consider. Several studies in the literature used different techniques for this choice, such as the global percentage error (GPE) [49] and the fuzzy multivariate algorithm [50].

In the study by [51], the authors proposed a strategy that would consider the use of two metrics for the optimal choice of the point in the multiobjective optimization applied to the vertical turning. Thus, from the calculation of the GPE, described in Eq. (5), and the entropy index proposed by [52], described in Eq. (6), we can obtain the optimal point of the Pareto frontier by calculating Eq. (7).

$$\text{GPE} = \sum_{i=1}^{m} \left| \frac{y_i^*}{T_i} - 1 \right|, \tag{5}$$

$$\begin{aligned} \text{Entropy} &= -\sum_{i=1}^{m} w_i \ln(w_i) \\ s.t. &: \; 0 \leq w_i \leq 1, \end{aligned} \tag{6}$$

$$\begin{cases} \text{Max} \;\; \xi = \dfrac{\text{Entropy}}{\text{GPE}} \\ St. : \sum_{i=1}^{m} w_i = 1 \\ 0 \le w_i \le 1, \end{cases} \tag{7}$$

where y_i^* is the value of the Pareto optimal responses; T_i are the defined targets; m is the number of targets.

3 NBI PCA-based approach to reduce dimensionality in optimization problems for LBM process

3.1 Materials

For the accomplishment of the experimental procedure, AISI 314S stainless steel of composition 0.25% C, 26% Cr-max, 47% Fe, 2% Mn, 22% Ni-max, 0.003% S, and 3% Si-max was used. This steel has wide applicability and was used in previous studies [15, 16]. This selection considered the technological application field, material suitability in precision mechanics, and micromold manufacturing. The workpiece is a small flat box with dimensions 10 mm × 10 mm × 0.1 mm, representative of the application field, and allows for the surface roughness measurement (Fig. 3).

The experiments were performed with the Deckel Maho Lasertec® machine; for LBM, model DML40SI was used (Fig. 4a). This equipment uses a Nd: YAG continuous laser. To perform data collection, a Mahr® rugosimeter was used; model M300 was connected to an RD18 measuring device (Fig. 4b).

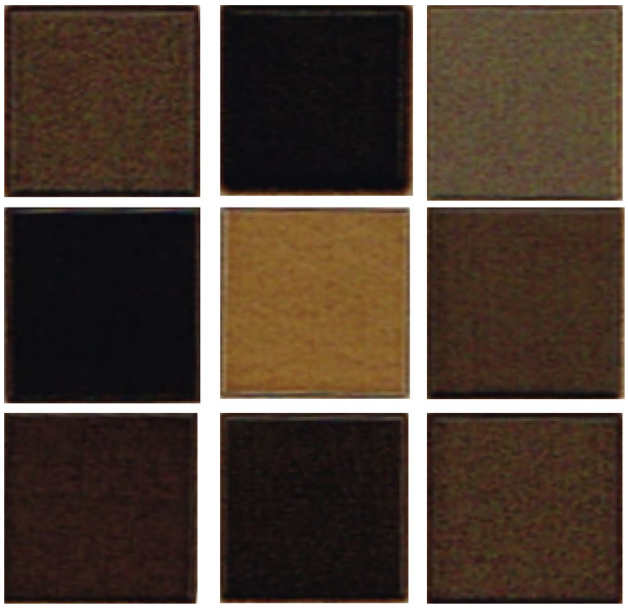

Fig. 3 Machined surface workpieces

3.2 Method

For this study, the process shown in the flowchart of Fig. 5 was followed. In Step 1, the DOE strategy must be applied to generate the experimental arrangement. Among the techniques, a CCD-type arrangement was used, which is a main type of response surface design. The limits of the main parameters of the LBM process [laser frequency—f (kHz); cutting speed—S (mm/min); and laser power—I (%)] were defined from preliminary tests, such that the chosen parameters are within the operational limits of the equipment. Table 1 shows the factorial, axial, and central levels of each parameter. From

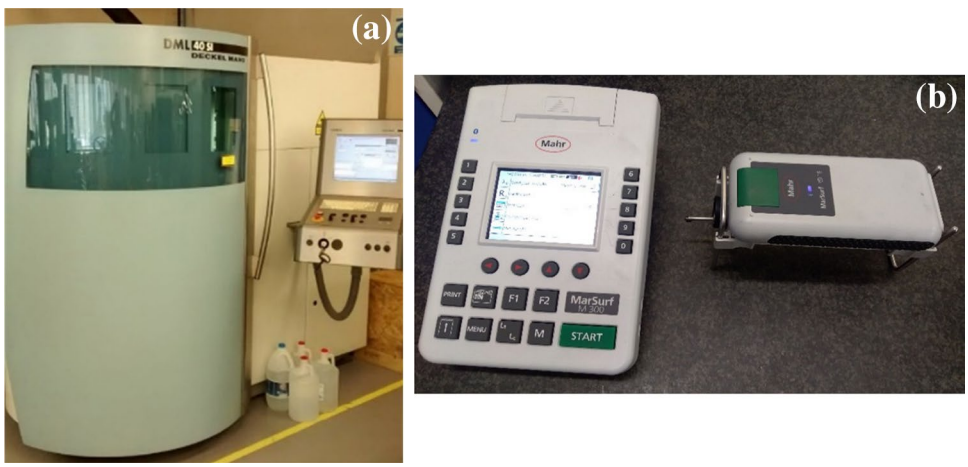

Fig. 4 **a** DML40SI LBM machine and **b** Mahr® M300 rugosimeter

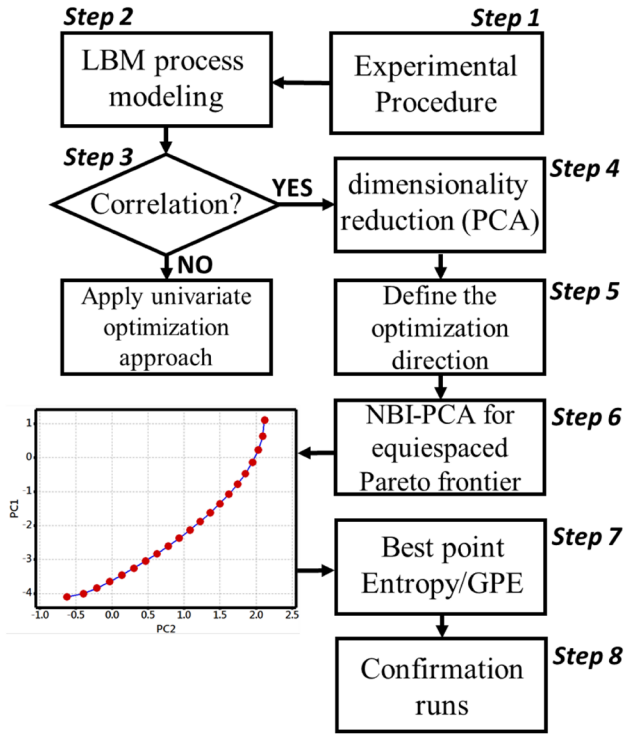

Fig. 5 Proposed application flowchart

Table 1 Input parameters and levels

Input parameters	Level				
	−1.682	−1	0	1	1.682
f [kHz]	11.2	15	20.5	26	29.7
S [mm/min]	29.5	200	450	700	870.4
I [%]	26.3	40	60	80	93.6

this, these parameters were designed according to a CCD, created for three factors at two levels with eight factorial points ($2^k = 2^3 = 8$), six axial points ($2k = 2 \times 3 = 6$) and six center points, totaling an experimental design of 20 runs. The experiments were performed randomly and the results are stored in Table 2. The roughness measurements are in µm and the MRR in cm^3/s. The parameter values were tested and chosen for a rough machining operation, where maximizing the MRR is the main target.

After completing the experiments and performing the data collection, one can continue with the applications of statistical and mathematical procedures highlighted in the flowchart of Fig. 5. These analyses are detailed in Sect. 4.

4 Results and discussion

4.1 LBM modeling

Following the model proposed in Fig. 5, after performing the experiments and collecting the responses, one must analyze the influence of the LBM process parameters on the quality characteristics analyzed (Step 2). Hence, one must use the second-order polynomial models developed using the RSM. The coefficient values of the quadratic function models were estimated using the ordinary least-squares algorithm, and shown in Table 3.

From the coefficients of the complete quadratic model, it is possible to verify that some terms are not significant for the model, that is, they are detrimental to the fit of the model. Therefore, the backward elimination strategy was applied to remove the non-significant term resulting in a new reduced model (bold values shown in Table 3), with R^2_{adj} equal to 69.29%, 68.97%, 79.42%, 79.6%, 72.93%, and 92.34% for quality characteristics R_a, R_q, R_z, R_p, R_t and MRR, respectively. According to [33], in a process that presents multiple quality characteristics, one should consider the variance–covariance structure of the data. To determine the best method to analyze the responses, correlation analysis was performed for roughness and MRR (Step 3), to determine if the process characteristics exhibit a multivariate nature and thus to use an appropriate technique. Table 4 presents the values of the Pearson coefficients and their respective p values. From this table, it can be verified that all the roughness responses (R_a, R_q, R_z, R_p, and R_t) present a high correlation, with Pearson values higher than 0.9. However, the MRR characteristic exhibits a lower correlation with the other characteristics analyzed, but with significant values for the multivariate study.

Owing to the significant correlations of the LBM process responses and its conflicting objectives, PCA can be used to reduce the response dimensionality and to analyze the correlated information adequately. Subsequently, the PCs found will be modeled and optimized by the NBI method to obtain the optimal points to solve the multiobjective problem.

4.2 Modeling and dimensionality reduction with PCA

Considering the multicorrelated structure of the quality characteristics, the PCA strategy is applied to reduce the dimensionality of the responses of interest (Step 4). The component scores, described in Table 2, can be extracted based on the correlation matrix. In addition, their respective eigenvectors and eigenvalues in Table 5 are verified. From this analysis, it is clear that the first two components

Table 2 Experimental matrix

Run	Setup			Responses						PCA	
	f	S	I	R_a	R_q	R_z	R_p	R_t	MRR	PC_1	PC_2
	[kHz]	[mm/min]	[%]	[μm]	[μm]	[μm]	[μm]	[μm]	[cm^3/s]		
1	15.00	200.00	40.00	4.54	5.85	31.30	14.46	39.58	5.95×10^{-4}	−1.38489	−0.67172
2	26.00	200.00	40.00	2.12	2.65	12.77	6.70	14.00	4.20×10^{-4}	−3.37942	−0.45119
3	15.00	700.00	40.00	7.27	9.03	42.06	22.59	47.90	7.81×10^{-4}	0.17639	−0.80031
4	26.00	700.00	40.00	3.68	4.53	17.47	8.82	18.86	4.21×10^{-4}	−2.67046	−0.63586
5	15.00	200.00	80.00	12.38	15.07	66.30	33.68	78.49	1.84×10^{-3}	3.51844	−0.08308
6	26.00	200.00	80.00	5.28	6.91	35.33	20.30	45.70	6.57×10^{-4}	−0.66515	−0.76341
7	15.00	700.00	80.00	11.82	14.66	63.70	31.40	79.66	2.05×10^{-3}	3.32004	0.26908
8	26.00	700.00	80.00	6.08	7.25	36.26	17.15	52.88	2.33×10^{-3}	0.04538	1.50940
9	11.25	450.00	60.00	11.93	14.93	61.52	33.55	80.09	1.77×10^{-3}	3.32695	−0.15310
10	29.75	450.00	60.00	3.14	4.71	14.96	8.04	17.93	1.21×10^{-3}	−2.56914	0.47979
11	20.50	29.55	60.00	11.91	15.91	69.30	33.67	95.14	2.24×10^{-4}	3.36421	−2.40146
12	20.50	870.45	60.00	3.07	4.14	26.24	12.64	30.49	1.24×10^{-3}	−1.91331	0.40748
13	20.50	450.00	26.36	3.64	4.36	17.57	8.68	22.42	3.07×10^{-4}	−2.67397	−0.79702
14	20.50	450.00	93.64	10.73	12.92	71.64	32.47	89.21	2.70×10^{-3}	3.62322	1.19121
15	20.50	450.00	60.00	6.22	7.62	36.61	17.18	47.00	1.54×10^{-3}	−0.26178	0.42284
16	20.50	450.00	60.00	5.90	7.38	36.71	17.81	42.50	1.57×10^{-3}	−0.36696	0.49336
17	20.50	450.00	60.00	6.17	7.51	36.35	16.91	38.37	1.56×10^{-3}	−0.44635	0.49681
18	20.50	450.00	60.00	6.23	7.71	36.14	18.10	41.29	1.56×10^{-3}	−0.31495	0.45018
19	20.50	450.00	60.00	5.88	7.55	36.52	17.95	44.76	1.58×10^{-3}	−0.30428	0.49439
20	20.50	450.00	60.00	6.17	7.60	35.60	17.33	38.25	1.60×10^{-3}	−0.42395	0.54260
Utopia point (ζ_{y_j})				9.921	12.009	58.678	28.201	72.060	2.77×10^{-3}	−4.1027	2.116

Table 3 Model coefficients for the RSM

	R_a	R_q	R_z	R_p	R_t	MRR	PC_1	PC_2
Constant	**6.1213**	**7.6045**	**36.5098**	**17.6221**	**42.3379**	$\mathbf{1.57\times10^{-3}}$	**−0.330130**	**0.481718**
f	**−2.4613**	**−2.9619**	**−13.1681**	**−6.7417**	**−16.0162**	$\mathbf{-1.74\times10^{-4}}$	**−1.626700**	**0.147133**
S	**−0.7571**	**−1.0843**	**−4.2929**	**−2.2368**	**−6.3849**	$\mathbf{2.77\times10^{-4}}$	**−0.446170**	**0.515182**
I	**2.1873**	**2.6527**	**13.8337**	**6.5888**	**18.2119**	**6.37×10−4**	**1.762310**	**0.500471**
f^2	0.3329	0.5104	−0.5515	0.6504	0.4454	-4.55×10^{-5}	0.109030	**−0.102384**
S^2	0.3166	0.5820	2.8179	1.4848	5.3262	$\mathbf{-3.14\times10^{-4}}$	0.231560	−0.512624
I^2	0.2090	0.0934	1.6989	0.5721	2.8513	-4.11×10^{-5}	0.142880	−0.090451
$f\times S$	0.0235	−0.0680	−0.3163	−0.8600	0.3187	$\mathbf{1.61\times10^{-4}}$	0.007080	**0.233071**
$f\times I$	−0.8550	−0.9845	−1.9113	−0.7615	−0.6187	-4.62×10^{-5}	−0.327110	0.021874
$S\times I$	−0.5073	−0.6405	−2.1412	−1.9600	−0.6037	$\mathbf{2.12\times10^{-4}}$	−0.219760	**0.367278**

Bold values represent the individually significant coefficients by backward elimination

are responsible for 98.5% of the explanation of variation structure from the six original analyzed responses (Table 5).

From the component scores (PC_1 and PC_2) described in Table 2, the response surface design is performed again to verify the coefficients and the regression model for the scores. Figure 6 presents the response surface graphs between the PCs and the input parameters obtained using the backward elimination strategy. The PC second-order models were obtained, and the R^2_{adj} values were calculated to $PC_1(\boldsymbol{x})$ equal to 77.78% and $PC_2(\boldsymbol{x})$ equal to 77.24%.

Figure 7 shows the dendrogram illustrating the similarity level between the analyzed responses and the components (Step 5). It is possible to verify that the first component ($PC_1(\boldsymbol{x})$) exhibits a higher similarity level with the roughness responses (R_a, R_q, R_z, R_p, and R_t); thus, it must be minimized. In an antagonistic sense, if $PC_2(\boldsymbol{x})$ presents a higher similarity level with the MRR, then it must be maximized.

Table 4 Correlation analysis for the LBM process characteristics

	R_a	R_q	R_z	R_p	R_t
R_q	0.996(1)				
	0.000(2)				
R_z	0.973(1)	0.969(1)			
	0.000(2)	0.000(2)			
R_p	0.979(1)	0.979(1)	0.989(1)		
	0.000(2)	0.000(2)	0.000(2)		
R_t	0.960(1)	0.962(1)	0.987(1)	0.976(1)	
	0.000(2)	0.000(2)	0.000(2)	0.000(2)	
MRR	0.460(1)	0.415(1)	0.500(1)	0.454(1)	0.462(1)
	0.041(2)	0.069(2)	0.025(2)	0.044(2)	0.040(2)

(1)Pearson correlation

(2)*P* value

4.3 Multivariate LBM process optimization by NBI approach

From the knowledge of optimization directions for the NBI application, one can generate the payoff *matrix* for the Utopia and Nadir score points, as shown in Eq. (8)

$$\mathbf{\Phi} = \begin{bmatrix} -4.103 & 1.099 \\ -0.626 & 2.116 \end{bmatrix}. \tag{8}$$

From the strategy presented in Sect. 2.3, in Step 6, the NBI method was applied using the generalized reduced gradient, where 0.05 was used as the weighting restriction to generate a Pareto frontier with 21 points. Figure 8 shows the equispaced Pareto frontier generated by NBI–PCA method and Table 6 presents the optimization data.

It is clear that the PCA and NBI combination resulted in an equispaced Pareto frontier, avoiding Pareto-optimal solutions agglomeration along the frontier. All 21 Pareto solutions can be considered optimal solutions. However, to determine the optimal point, the entropy/GPE criterion was used (Step 7) through Eqs. (5), (6), and (7). Table 6 shows the values found for the entropy/GPE method.

Considering the highest value for the entropy/GPE relation, we obtained the value of 0.119, representing, in the original quality characteristics, $\boldsymbol{Y} = [5.56; 6.8; 34.1; 16.48; 37.79; 1.91 \times 10^{-3}]$ for R_a, R_q, R_z, R_p, R_t, and *MRR*,

Table 5 PCA applied to LBM responses

Eigenvalue	5.1604	0.7522	0.0593	0.0189	0.007	0.0023
Proportion	0.860	0.125	0.010	0.003	0.001	0.000
Cumulative	**0.860**	**0.985**	0.995	0.998	1.000	1.000
Variable	Eigenvectors					
	PC_1	PC_2	PC_3	PC_4	PC_5	PC_6
R_a	**0.434**	**−0.107**	0.527	0.122	0.202	0.683
R_q	**0.432**	**−0.165**	0.487	0.256	−0.136	−0.682
R_z	**0.437**	**−0.052**	−0.351	−0.232	0.768	−0.201
R_p	**0.435**	**−0.114**	−0.099	−0.728	−0.504	0.061
R_t	**0.432**	**−0.096**	−0.591	0.58	−0.307	0.154
MRR	**0.239**	**0.968**	0.052	0.016	−0.05	−0.029

The values in bold represent the principal components that will be used in the study

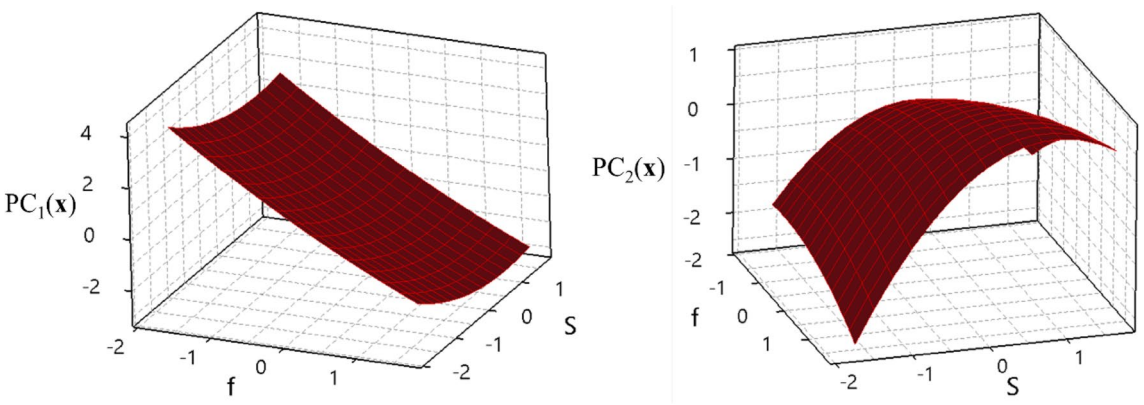

Fig. 6 Response surfaces to PC_1 and PC_2

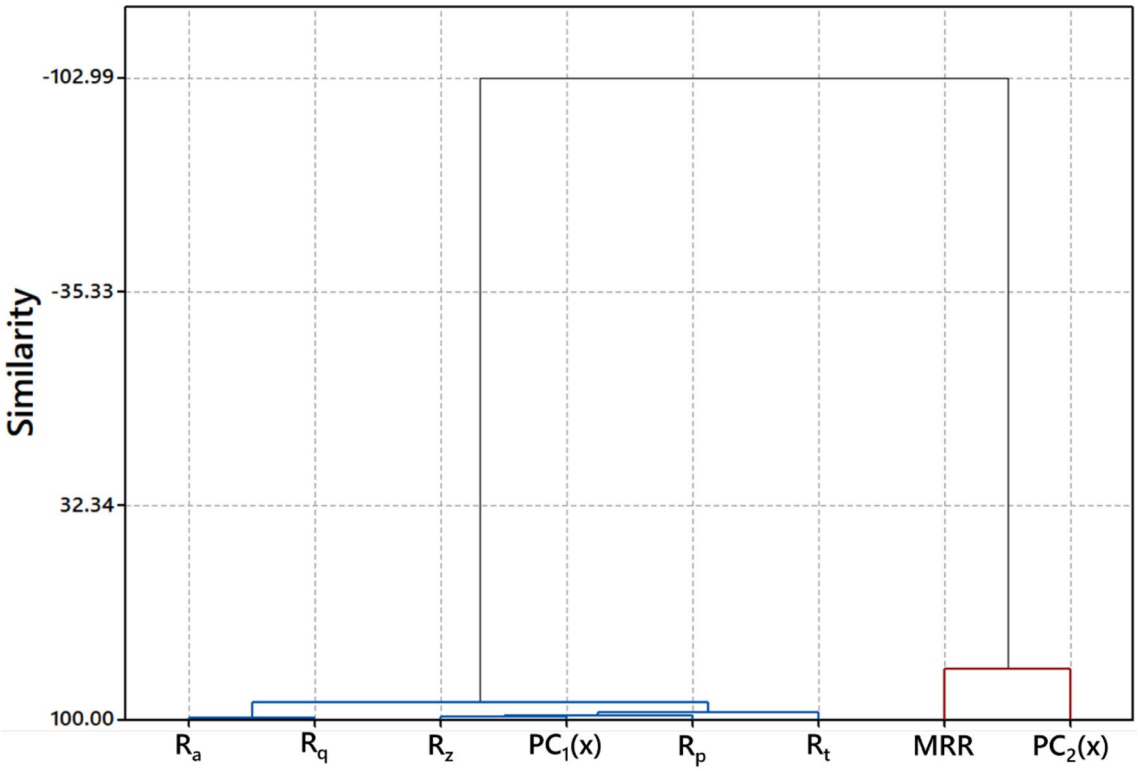

Fig. 7 Dendrogram of absolute correlation coefficient distance

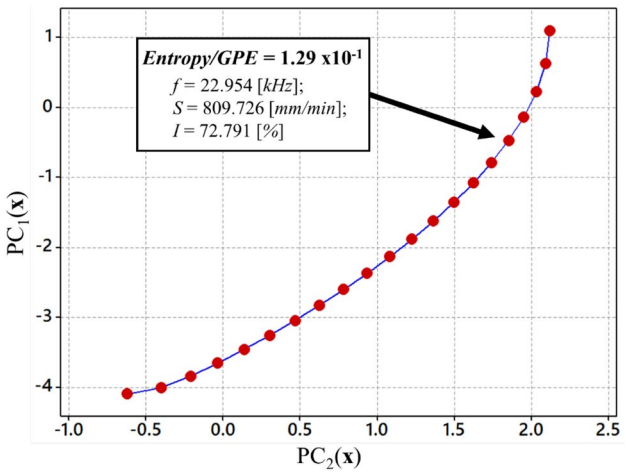

Fig. 8 Pareto frontier between PC_1 and PC_2

respectively. The machine input parameters for this point are $\boldsymbol{x}^*_{\text{code}} = [0.591; 1.439; 0.639]$, representing $f = 22.95$ (kHz), $S = 809.73$ (mm/s), and $I = 72.79$ (%). The dimensionless values of the scores of the components were $PC_1 = -0.476$ and $PC_2 = 1.849$.

4.4 Confirmation runs

To prove the LBM multivariate optimization application efficiency, an 80% test power confirmation experiment was designed, totalizing five confirmation experiments. Starting from the Pareto frontier optimum point, the experiments were performed with the following machine input parameters $\boldsymbol{x}^*_{\text{uncoded}} = [22.95; 809.73; 72.79]$. The confirmation runs (Step 8) are shown in Table 7.

Finally, to verify if a statistical difference exists between the confirmatory runs, a hypothesis test was performed. Because the null hypothesis (values are equal) is not rejected, i.e., no significant difference exists between the confirmation experiments and the optimal point found in the optimization, the efficiency of the method is proven. The established multivariate confidence intervals are presented in Table 7.

5 Performance of the NBI method for LBM process without dimensionality reduction

To demonstrate the performance of the NBI method without reducing the dimensionality of the data through the multivariate PCA strategy, optimization was performed for all quality characteristics simultaneously. With this

Table 6 Optimal solutions for NBI–PCA approach

β_1	β_2	Uncoded setup			NBI-PCA approach response optmization								
		f	S	I	R_a	R_q	R_z	R_p	R_t	MRR	PC_1	PC_2	Entropy/GPE
		[kHz]	[mm/min]	[%]	[μm]	[μm]	[μm]	[μm]	[μm]	[cm^3/s]			
0.00	1.00	21.181	751.646	82.950	7.723	9.450	46.802	22.740	54.204	2.43×10^{-3}	1.099733	2.116125	1.72×10^{-8}
0.05	0.95	21.758	774.560	80.192	7.067	8.643	42.980	20.848	49.258	2.29×10^{-3}	0.627975	2.09057	9.43×10^{-2}
0.10	0.90	22.219	790.548	77.616	6.510	7.959	39.710	19.235	45.027	2.15×10^{-3}	0.222474	2.030089	1.20×10^{-1}
0.15	0.85	22.612	801.846	75.164	6.015	7.353	36.787	17.797	41.249	2.03×10^{-3}	−0.1414	1.947665	1.28×10^{-1}
0.20	**0.80**	**22.954**	**809.726**	**72.791**	**5.563**	**6.801**	**34.109**	**16.484**	**37.791**	$\mathbf{1.91\times10^{-3}}$	**−0.4758**	**1.84973**	$\mathbf{1.29\times10^{-1}}$
0.25	0.75	23.256	814.893	70.469	5.145	6.292	31.618	15.265	34.577	1.80×10^{-3}	−0.78798	1.740039	1.26×10^{-1}
0.30	0.70	23.526	817.730	68.184	4.753	5.816	29.277	14.122	31.557	1.69×10^{-3}	−1.08242	1.621016	1.21×10^{-1}
0.35	0.65	23.769	818.483	65.920	4.383	5.368	27.058	13.042	28.698	1.58×10^{-3}	−1.36232	1.494326	1.14×10^{-1}
0.40	0.60	23.990	817.261	63.671	4.033	4.945	24.943	12.015	25.976	1.48×10^{-3}	−1.62995	1.361173	1.07×10^{-1}
0.45	0.55	24.190	814.085	61.431	3.699	4.543	22.919	11.034	23.374	1.38×10^{-3}	−1.88702	1.222451	9.86×10^{-2}
0.50	0.50	24.370	809.079	59.179	3.379	4.160	20.976	10.096	20.877	1.29×10^{-3}	−2.1348	1.078838	9.02×10^{-2}
0.55	0.45	24.531	802.086	56.915	3.073	3.794	19.105	9.195	18.477	1.19×10^{-3}	−2.3743	0.930853	8.15×10^{-2}
0.60	0.40	24.674	792.990	54.628	2.780	3.445	17.302	8.329	16.168	1.11×10^{-3}	−2.60624	0.778884	7.26×10^{-2}
0.65	0.35	24.800	781.568	52.307	2.499	3.113	15.562	7.498	13.945	1.02×10^{-3}	−2.83113	0.623204	6.37×10^{-2}
0.70	0.30	24.908	767.422	49.945	2.230	2.797	13.886	6.700	11.808	9.40×10^{-4}	−3.04928	0.463968	5.47×10^{-2}
0.75	0.25	24.995	750.082	47.515	1.975	2.498	12.274	5.938	9.760	8.62×10^{-4}	−3.2607	0.301184	4.56×10^{-2}
0.80	0.20	25.060	728.601	45.003	1.733	2.219	10.734	5.214	7.812	7.87×10^{-4}	−3.46499	0.134641	3.66×10^{-2}
0.85	0.15	25.107	701.341	42.399	1.508	1.965	9.278	4.538	5.988	7.16×10^{-4}	−3.66094	−0.03629	2.75×10^{-2}
0.90	0.10	25.133	665.246	39.672	1.306	1.744	7.942	3.926	4.341	6.50×10^{-4}	−3.84545	−0.21327	1.84×10^{-2}
0.95	0.05	25.176	612.848	36.914	1.142	1.580	6.821	3.429	3.031	5.92×10^{-4}	−4.00888	−0.40134	9.26×10^{-3}
1.00	0.00	25.606	526.852	35.697	1.057	1.536	6.322	3.217	2.740	5.71×10^{-4}	−4.10266	−0.62614	0.000

The values in bold represent the optimal point found by the method

Table 7 Confirmation runs for NBI–PCA approach for LBM

Run	R_a [μm]	R_q [μm]	R_z [μm]	R_p [μm]	R_t [μm]	MRR [cm^3/s]
1	5.61	6.86	35.92	16.82	40.46	1.98×10^{-3}
2	5.69	7.18	36.57	17.37	41.13	1.96×10^{-3}
3	5.6	6.91	34.67	16.77	39.8	1.92×10^{-3}
4	5.58	6.9	34.54	16.63	39.67	1.95×10^{-3}
5	5.61	6.88	35.01	16.52	39.22	1.94×10^{-3}
Mean	**5.618**	**6.946**	**35.342**	**16.822**	**40.056**	$\mathbf{1.950\times10^{-3}}$
SD	4.21×10^{-2}	1.32×10^{-1}	8.73×10^{-1}	3.28×10^{-1}	7.47×10^{-1}	2.24×10^{-2}
[a]CI UB	5.721	7.269	37.478	17.625	41.883	2.005×10^{-3}
Pareto	5.563	6.801	34.109	16.484	37.791	1.91×10^{-3}
[b]CI LB	5.515	6.623	33.206	16.019	38.23	1.895×10^{-3}

The values in bold represent the mean values found in the confirmation experiment

[a]*CI UB* multivariate upper bound for confidence interval

[b]*CI LB* lower bound

application, without considering the multicorrelated structure of the data in the calculations, the six interest responses were analyzed, thus generating a high number of NBI subproblems, i.e., a total of 259. Using the entropy/GPE method to obtain the optimal point, it was observed that the main interest response (MRR), presented a lower value than that obtained by the NBI–PCA method.

Thus, comparing the best results of each approach, it can be inferred that the multivariate method yielded a better MRR value. This result was expected, because the data present a variance–covariance structure that should be

considered, considering the multivariate data. In addition, the multivariate method provides a significant contribution in computational effort to obtain the optimal solutions, because it presents a smaller subproblem number, with a 91.89% reduction (from 259 to 21 subproblems).

6 Conclusion

LBM is a promising machining method owing to non-contact material removal, high precision machining, and no tool wear. As it is an expensive process and presents many quality responses, this study proposed a multivariate approach to optimize the LBM process to reduce the dimensionality of the problems and to obtain an optimal solution. In view of the correlated data structure, it was possible to apply a multivariate strategy to reduce the dimensionality of the optimization problems. The RMS methodology and NBI optimization method were also used to provide a smaller number of experiments and an equispaced Pareto frontier. Therefore, the following conclusions can be drawn:

- The proposed approach yielded an optimal point in $\boldsymbol{x}^* =$ [22.95 kHz; 809.73 mm/s; 72.79%]. These results provided an optimum value for the responses, with the MRR equal to 0.639 cm^3/s and the roughness $R_a = 5.56\ \mu_m$; $R_q = 6.8\ \mu_m$; $R_z = 34.1\ \mu_m$; $R_p = 16.48\ \mu_m$; $R_t = 37.79\ \mu_m$.
- The NBI–PCA approach applied to LBM provided a dimensional reduction of the problem; simultaneously, it promoted a smaller number of optimization subproblems (from 259 to 21 subproblems), and a 91.89% reduction.
- The optimal parameters determined by the NBI–PCA approach were verified by confirmation runs. The results were presented within the multivariate confidence intervals, evidencing the method capability when applied to LBM.

Acknowledgements The authors gratefully acknowledge the IDMEC/UL, Associated Laboratory for Energy, Transports and Aeronautics (LAETA), IST/University of Lisbon, the SMART2 program from ERASMUS MUNDUS, FAPEMIG, CAPES, CNPq and IFSULDEMINAS.

References

1. Meijer J (2004) Laser beam machining (LBM), state of the art and new opportunities. J Mater Process Technol 149:2–17. https://doi.org/10.1016/j.jmatprotec.2004.02.003
2. Dubey AK, Yadava V (2008) Laser beam machining-A review. Int J Mach Tools Manuf 48:609–628. https://doi.org/10.1016/j.ijmachtools.2007.10.017
3. Gomes GF, de Almeida FA, da Silva Lopes Alexandrino P et al (2018) A multiobjective sensor placement optimization for SHM systems considering Fisher information matrix and mode shape interpolation. Eng Comput 10:1–17. https://doi.org/10.1007/s00366-018-0613-7
4. Saghatforoush A, Monjezi M, Shirani Faradonbeh R, Jahed Armaghani D (2016) Combination of neural network and ant colony optimization algorithms for prediction and optimization of flyrock and back-break induced by blasting. Eng Comput 32:255–266. https://doi.org/10.1007/s00366-015-0415-0
5. Chen XL, Fu JP, Yao JL, Gan JF (2018) Prediction of shear strength for squat RC walls using a hybrid ANN–PSO model. Eng Comput 34:367–383. https://doi.org/10.1007/s00366-017-0547-5
6. Gomes GF, de Almeida FA, da Cunha SS et al (2018) An estimate of the location of multiple delaminations on aeronautical CFRP plates using modal data inverse problem. Int J Adv Manuf Technol 99:1155. https://doi.org/10.1007/s00170-018-2502-z
7. MiarNaeimi F, Azizyan G, Rashki M (2017) Multi-level cross entropy optimizer (MCEO): an evolutionary optimization algorithm for engineering problems. Eng Comput. https://doi.org/10.1007/s00366-017-0569-z
8. Gomes GF, da Cunha SS, Ancelotti AC (2018) A sunflower optimization (SFO) algorithm applied to damage identification on laminated composite plates. Eng Comput. https://doi.org/10.1007/s00366-018-0620-8
9. Dubey A, Yadava V (2008) Robust parameter design and multi-objective optimization of laser beam cutting for aluminium alloy sheet. Int J Adv Manuf Technol 38:268–277. https://doi.org/10.1007/s00170-007-1105-x
10. Kasman Ş, Etem Saklakoglu I (2012) Determination of process parameters in the laser micromilling application using Taguchi method: a case study for AISI H13 tool steel. Int J Adv Manuf Technol 58:201–209. https://doi.org/10.1007/s00170-011-3371-x
11. Ghosal A, Manna A (2013) Optics & laser technology response surface method based optimization of ytterbium fiber laser parameter during machining of Al/ Al_2O_3 -MMC. Opt Laser Technol 46:67–76. https://doi.org/10.1016/j.optlastec.2012.04.030
12. Parandoush P, Hossain A (2014) A review of modeling and simulation of laser beam machining. Int J Mach Tools Manuf 85:135–145. https://doi.org/10.1016/j.ijmachtools.2014.05.008
13. Li CH, Tsai MJ (2009) Multi-objective optimization of laser scribing for the isolation process of solar cell wafers using grey relational analysis. IEEE Int Symp Ind Electron 41:1154–1159. https://doi.org/10.1109/ISIE.2009.5218137
14. Teixidor D, Ferrer I, Ciurana J, Özel T (2013) Optimization of process parameters for pulsed laser milling of micro-channels on AISI H13 tool steel. Robot Comput Integr Manuf 29:209–218
15. Childs THC, Hauser C, Badrossamay M (2004) Mapping and modelling single scan track formation in direct metal selective laser melting. CIRP Ann Manuf Technol 53:191–194. https://doi.org/10.1016/S0007-8506(07)60676-3
16. Childs THC, Hauser C, Badrossamay M (2005) Selective laser sintering (melting) of stainless and tool steel powders: experiments and modelling. Proc Inst Mech Eng Part B J Eng Manuf 219:339–357
17. Pandey AK, Dubey AK (2012) Taguchi based fuzzy logic optimization of multiple quality characteristics in laser cutting of Duralumin sheet. Opt Lasers Eng 50:328–335. https://doi.org/10.1016/j.optlaseng.2011.11.005
18. Mistry V, James S (2017) Finite element analysis and simulation of liquid-assisted laser beam machining process. Int J Adv Manuf Technol 2325–2331. https://doi.org/10.1007/s00170-017-1009-3
19. Darwish S, Ahmed N, Alahmari AM, Mufti NA (2017) A study of micro-channel size and spatter dispersion for laser beam micro-milling. Mater Manuf Process 32:171–184. https://doi.org/10.1080/10426914.2016.1176188

20. Darwish S, Ahmed N, Alahmari AM, Mufti NA (2016) A comparison of laser beam machining of micro-channels under dry and wet mediums. Int J Adv Manuf Technol 83:1539–1555. https://doi.org/10.1007/s00170-015-7658-1
21. Pan LK, Wang CC, Wei SL, Sher HF (2007) Optimizing multiple quality characteristics via Taguchi method-based Grey analysis. J Mater Process Technol 182:107–116. https://doi.org/10.1016/j.jmatprotec.2006.07.015
22. Schweier M, Heins JF, Haubold MW, Zaeh MF (2013) Spatter formation in laser welding with beam oscillation. Phys Procedia 41:20–30. https://doi.org/10.1016/j.phpro.2013.03.047
23. Rao RV, Kalyankar VD (2014) Optimization of modern machining processes using advanced optimization techniques: a review. Int J Adv Manuf Technol 73:1159–1188. https://doi.org/10.1007/s00170-014-5894-4
24. Almeida FA de, Gomes GF, De Paula VR et al (2018) A weighted mean square error approach to the robust optimization of the surface roughness in an AISI 12L14 free-machining steel-Turning process. Stroj Vestnik/J Mech Eng 64:147–156. https://doi.org/10.5545/sv-jme.2017.4901
25. Yu X, Zhang S, Johnson E (2003) A discrete post-processing method for structural optimization. Eng Comput 19:213–220. https://doi.org/10.1007/s00366-003-0259-x
26. Almeida FA, Gomes GF, Sabioni RC, Gomes JHF, Paula VR, Paiva AP et al (2018) A gage study applied in shear test to indentify variation causes from a resistance spot welding measurement system. Stroj Vestnik/J Mech Eng 63:621–631
27. Fabiano Luis N, Tayana Incerti P, Pedro Paulo B et al (2017) Multivariate normal boundary intersection based on rotated factor scores: a multiobjective optimization method for methyl orange treatment. J Clean Prod 143:413–439
28. Manjoth S, Keshavamurthy R, Kumar GSP (2016) Optimization and analysis of laser beam machining parameters for Al7075-TiB < inf> 2</inf> in-situ composite. IOP Conf Ser Mater Sci Eng 149:12013. https://doi.org/10.1088/1757-899X/149/1/012013
29. Ahmed N, Alahmari AM, Darwish S, Khan AA (2016) Experimental investigation of micro-channels produced in aluminum alloy (AA 2024) through laser machining. Appl Phys A 122:948. https://doi.org/10.1007/s00339-016-0463-3
30. Umer U, Mohammed MK, Al-Ahmari A (2017) Multi-response optimization of machining parameters in micro milling of alumina ceramics using Nd:YAG laser. Meas J Int Meas Confed 95:181–192. https://doi.org/10.1016/j.measurement.2016.10.004
31. Prakash C, Kansal HK, Pabla BS, Puri S (2016) Multi-objective optimization of powder mixed electric discharge machining parame- ters for fabrication of biocompatible layer on β -Ti alloy using NSGA-II coupled with Taguchi based response surface methodology †. J Mech Sci Technol 30:4195–4204. https://doi.org/10.1007/s12206-016-0831-0
32. Costa DMD, Belinato G, Brito TG et al (2016) Weighted principal component analysis combined with Taguchi's Signal-to-noise ratio to the multiobjective optimization of dry end milling process: a comparative study. J Brazilian Soc Mech Sci Eng. https://doi.org/10.1007/s40430-016-0614-7
33. Almeida FA, De Paula TI, Leite RR, Gomes GF, Gomes JHF, Paiva APBP (2018) A multivariate GR&R approach to variability evaluation of measuring instruments in resistance spot welding process. J Manuf Process 36:465–479. https://doi.org/10.1016/j.jmapro.2018.10.030
34. Montgomery DC (2016) Design and analysis of experiments, 9th edn. Wiley, New York
35. Myers RH, Montgomery DC, Anderson-Cook CM (2009) Response surface methodology, 3rd ed. Taylor & Francis, Routledge
36. Singh D, Rao PV (2007) A surface roughness prediction model for hard turning process. Int J Adv Manuf Technol 32:1115–1124
37. Skrypnyk R, Nielsen JCO, Ekh M, Pålsson BA (2018) Metamodelling of wheel–rail normal contact in railway crossings with elasto-plastic material behaviour. Eng Comput. https://doi.org/10.1007/s00366-018-0589-3
38. Amaral FF, Almeida FA, Costa SC, Leme RCPA (2018) Application of the response surface methodology for optimization of the resistance spot welding process in AISI 1006 galvanized steel. Soldag Inspeção 32:129–142
39. Camposeco-Negrete C (2015) Optimization of cutting parameters using response surface method for minimizing energy consumption and maximizing cutting quality in turning of AISI 6061 T6 aluminum. J Clean Prod 91:109–117
40. Asiltürk I, Neşeli S, Ince MA (2016) Optimisation of parameters affecting surface roughness of Co28Cr6Mo medical material during CNC lathe machining by using the Taguchi and RSM methods. Measurement 78:120–128
41. Cukor G, Jurković Z, Sekulić M (2011) Rotatable central composite design of experiments versus Taguchi method in the optimization of turning. Metalurgija 50:17–20
42. Al-Ahmari AMA (2007) Predictive machinability models for a selected hard material in turning operations. J Mater Process Technol 190:305–311
43. Noordin MY, Venkatesh VC, Sharif S et al (2004) Application of response surface methodology in describing the performance of coated carbide tools when turning AISI 1045 steel. J Mater Process Technol 145:46–58
44. Johnson RA, Wichern DW (2007) Applied multivariate statistical analysis, 6th edn. Prentice Hall, New Jersey
45. Das I, Dennis JE (1998) Normal-boundary intersection: a new method for generating the pareto surface in nonlinear multicriteria optimization problems. SIAM J Optim 8:631–657. https://doi.org/10.1137/S1052623496307510
46. Brito TG, Paiva AP, Ferreira JR et al (2014) A normal boundary intersection approach to multiresponse robust optimization of the surface roughness in end milling process with combined arrays. Precis Eng 38:628–638. https://doi.org/10.1016/j.precisioneng.2014.02.013
47. Lopes LGD, Brito TG, Paiva AP et al (2016) Robust parameter optimization based on multivariate normal boundary intersection. Comput Ind Eng 93:55–66. https://doi.org/10.1016/j.cie.2015.12.023
48. Abdollah A, Hadi M, Ali Esmaeel N et al (2015) Multi-objective economic emission dispatch considering combined heat and power by normal boundary intersection method..2015.07.011. Electr Power Syst Res 129:32–43
49. Gomes JHF, Paiva a P, Costa SC et al (2013) Weighted Multivariate Mean Square Error for processes optimization: a case study on flux-cored arc welding for stainless steel claddings. Eur J Oper Res 226:522–535. https://doi.org/10.1016/j.ejor.2012.11.042
50. Gaudêncio JHD, Almeida FA, Sabioni RC, Turrioni JB, Paiva AP, Campos PHS (2018) Fuzzy multivariate mean square error in equispaced pareto frontiers considering manufacturing process optimization problems. Eng Comput. https://doi.org/10.1007/s00366-018-0660-0
51. Rocha LCS, De Paiva AP, Balestrassi PP et al (2015) Entropy-based weighting for multiobjective optimization: an application on vertical turning. Math Probl Eng. https://doi.org/10.1155/2015/608325
52. Shannon CE (1948) A mathematical theory of communication. Bell Syst Tech J 27:379–423